Improved scatterer size estimation using backscatter coefficient measurements with coded excitation and pulse compression

Steven G. Kanzler[a] and Michael L. Oelze[b]
Bioacoustics Research Laboratory, Department of Electrical and Computer Engineering, University of Illinois at Urbana-Champaign, Urbana, Illinois 61801

(Received 27 August 2007; revised 17 March 2008; accepted 19 March 2008)

Scatterer size estimates from ultrasonic backscatter coefficient measurements have been used to differentiate diseased tissue from normal. A low echo signal-to-noise ratio (eSNR) leads to increased bias and variance in scatterer size estimates. One way to improve the eSNR is to use coded excitation (CE). The normalized backscatter coefficient was measured from three tissue-mimicking phantoms by using CE and conventional pulsing (CP) techniques. The three phantoms contained randomly spaced glass beads with median diameters of 30, 45, and 82 μm, respectively. Measurements were made with two weakly focused, single-element transducers (f_0=5 MHz and f_0=10 MHz). For CE, a linear frequency modulated chirp with a time bandwidth product of 40 was used and pulse compression was accomplished by the use of a Wiener filter. Preliminary results indicated that improved estimation bias versus penetration depth was obtained by using CE compared to CP. The depth of penetration, where the accuracy of scatterer diameter estimates (absolute divergence $<$25%) were obtained with the 10 MHz transducer, was increased up to 50% by using CE versus CP techniques. In addition, for a majority of the phantoms, the increase in eSNR from CE resulted in a modest reduction in estimate variance versus depth of penetration.
 [DOI: 10.1121/1.2908293]

PACS number(s): 43.80.Vj [FD] Pages: 4599–4607

I. INTRODUCTION

The radio frequency (rf) spectrum of ultrasonic backscatter contains information that can be used to noninvasively characterize the structural and mechanical properties of tissue. Imaging techniques based on quantifying the ultrasonic backscatter have been successfully used to diagnose and monitor disease, such as cancer, in clinical settings. Furthermore, these imaging approaches have been used to differentiate different kinds of tissues.[1–5] Parametric images enhanced by scatterer parameters, i.e., the average scatterer size and acoustic concentration, have been constructed for test phantoms[6] and tissues.[7] In clinical settings, these imaging techniques have been successful in diagnosing prostate cancer, ocular tumors, and cardiac and vascular abnormalities.[1,8–10]

Because of the weak scattering condition in tissues, the backscattered signals often have low echo signal-to-noise ratio (eSNR). eSNR specifically refers to the ratio of the echo signals from ultrasonic scatter to background noise (i.e., electronic noise).[11] As with any estimation scheme, low eSNR leads to increased bias and variance in scatterer size estimates.[12] To improve the eSNR, either the amplitude or the pulse duration of the transmitted sound wave can be increased. However, the maximum pressure amplitude (or maximum negative peak pressure level of the propagating sound wave) that can be transmitted into a biological medium is limited because of the possibility of bioeffects.[13] Because of the possibility of bioeffects in diagnostic ultrasound, ultrasonic imaging devices are limited in the United States by the Food and Drug Administration to a spatial peak temporal average intensity of 720 mW/cm^2 and a mechanical index (MI$<$1.9), where the MI is the rarefactional pressure in Megapascals divided by the square root of the frequency in Megahertz.[14] As a result of this pressure amplitude limit, in many cases, the penetration depth can only be increased safely by increasing the pulse duration.[15] However, increasing the duration of the excitation waveform would cause a decrease in axial resolution.

A method to increase the pulse duration while retaining the spatial resolution is through coded excitation and pulse compression. Coded excitation was first used in radar applications to increase the signal energy.[16] Coded signals of long duration were used to excite the source and then the received echoes were filtered or compressed to restore the spatial resolution of the system. Examples of coded excitation schemes that have been used with pulse compression include binary codes, such as Barker codes or Golay codes, or frequency modulated (FM) waveforms, also known as chirps.[17]

In the current study, coded excitation using pulse compression (CEPC) has been used to increase the eSNR of signals backscattered from tissue-mimicking phantoms. Scatterer size estimates were then obtained from the backscattered waveforms by using CEPC and conventional pulsing (CP) techniques and compared. Specifically, linear FM chirps were used as the coded excitation waveform. Section II discusses the methodology of the experimental setup and the implementation of the CEPC routines. Results of the experimental measurements are given in Sec. III. Discussion of the results and some final conclusions are given in Sec. IV.

[a]Also at Department of Engineering and Natural Sciences, University of Applied Sciences, Merseburg 06217, Germany.
[b]Electronic mail: oelze@uiuc.edu

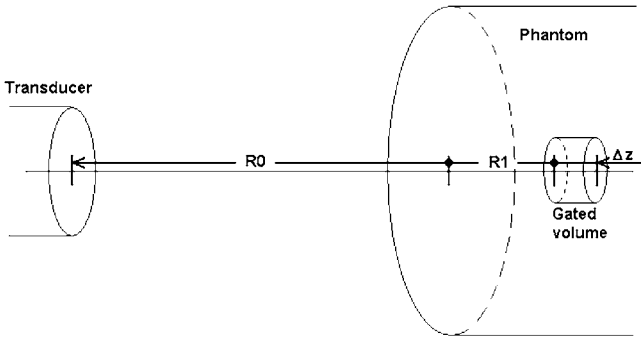

FIG. 1. The distance between the surface of the transducer and the surface of the phantom is R_0, the distance from the the surface of the phantom to the surface of the ROI is R_1, and the length of the gated region is Δz. The focal depth is at R_0+R_1.

II. METHODS AND MATERIALS

A. Experimental setup

Weakly focused ($f/3$ and $f/4$, respectively) single-element transducers were placed in a tank filled with degassed water (21 °C). The first transducer had a nominal center frequency of 5 MHz ($f/3$) and a −6 dB bandwidth of 84% estimated from a pulse-excited signal reflected from a planar surface. The second transducer had a nominal center frequency of 10 MHz ($f/4$) and a 91% −6 dB bandwidth estimated from a pulse-excited signal reflected from a planar surface. The −6 dB depth of field (DOF) and beam width of the transducers were measured by using the wire technique.[18] The −6 dB DOFs were estimated to be 9.1 and 16.9 mm for the 5 and 10 MHz sources, respectively. The −6 dB beam widths were estimated to be 850 and 613 μm for the 5 and 10 MHz transducers, respectively. The transducers were used to measure the backscatter from tissue-mimicking (TM) phantoms. In experiments, a TM phantom was placed in a tank of degassed water. The transducer was positioned so that the beam axis was perpendicular to the face of the phantom and the focus of the transducer was inside the surface of the phantom.

Figure 1 shows the geometry of the transducer and the phantom. For the experiment by using CP [Fig. 2(a)], the transducer was excited by a Panametrics 5800 pulser/receiver (Waltham, MA) and connected through a diplexer (Ritec, Warwick, RI). For the experiment by using CEPC [Fig. 2(b)], the transducer was excited by an arbitrary waveform generator (AWG) (Tabor Electronics WW1281, Tel Hanan, Israel) with a sampling frequency of 100 MHz. From the AWG, the signal was amplified by a 50 dB rf power amplifier (ENI 325LA, Rochester, NY). The amplified signal was connected to the transducer through the diplexer. For both experiments, the backscattered echo signals were received by a Panametrics 5900 pulser/receiver (Waltham, MA) through the diplexer and then acquired by a 12 bit analog-to-digital (A/D) card (Strategic Test UF3025, Akersberga-Stockholm, Sweden) and recorded on the hard drive of a personal computer. The backscattered power spec-

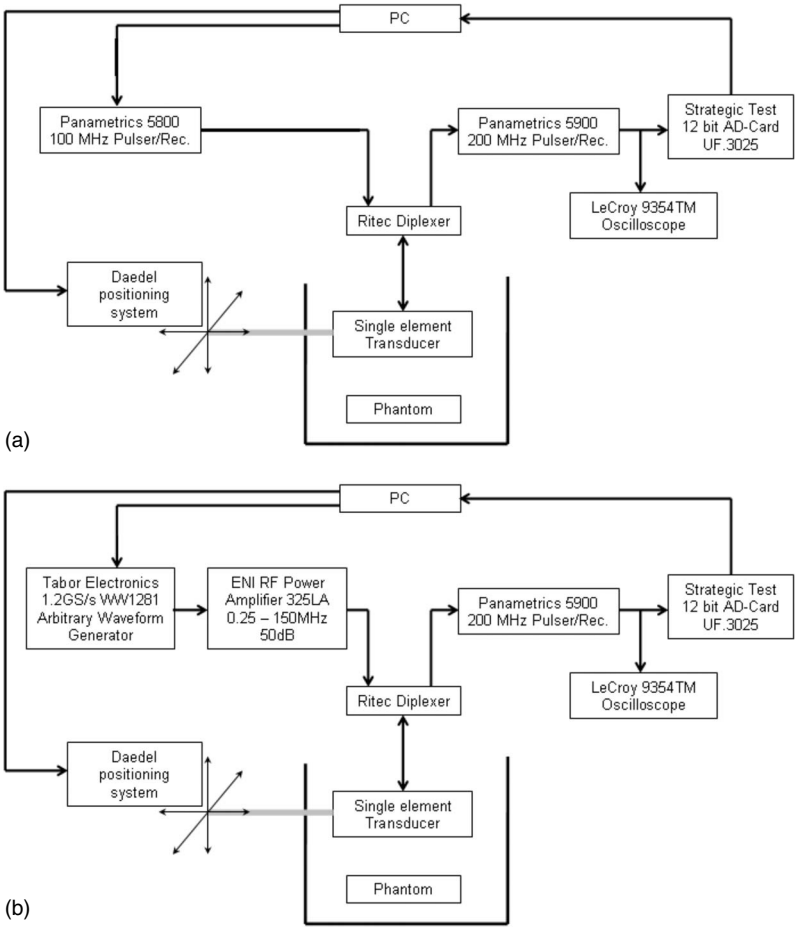

FIG. 2. Block diagram of experimental setup with (a) CP method and (b) CEPC method.

trum was estimated from the backscattered ultrasonic signals and normalized by a reference spectrum.[1] To obtain the reference waveform, a planar surface (Plexiglas®) was placed perpendicular to the beam axis with the surface near the focus of the transducer and the reflected signal recorded.

The A/D card is limited to a voltage range of ±1 V with a dynamic range of 12 bit. However, the amplitude of the reflection from the front surface of the phantom was large compared to the amplitude of the speckle corresponding to inside the phantom. Often, the difference in the signal amplitude from the front surface of the phantom compared to the speckle within the phantom was larger than the dynamic range available to the system. A gain was applied to the backscattered signal through the Panametrics 5900. As a result, the signal corresponding to the reflection off the front surface was clipped to ±1 V; however, the signal corresponding to the speckle more fully spanned the dynamic range of the A/D card. When CP was used, the clipping did not influence the measurements or subsequent scatterer diameter estimates. However, clipping the signal did influence the ability to compress the backscattered signals by using CEPC. During the acquisition process, the A/D card transformed the linear FM chirp (FM sinusoidal waveform), resulting from the reflection off the front surface of the phantom into a pseudochirp (FM rectangular waveform) by clipping the data above 1 V and below −1 V. Because the scattered signal is often −40 dB or more below the signal reflected from the front surface and the dynamic range of the A/D card was 12 bit, the signal reflected from the front surface was allowed to clip rather than attenuate the whole signal. As a result, the dynamic range of the A/D card was used to span the scattered signal. Rectangular waveforms contain high frequency content because of the sharp edges, and this causes side lobes of high amplitudes after compression. To avoid these side lobes, the portion of the echo signal containing the pseudochirp was replaced by artificially created zero-mean white Gaussian noise (WGN) with the same variance as the system noise. The variance of the system noise was estimated from recordings in the region without scatterers (noise window) and was used in subsequent estimates of eSNR. The eSNR value was determined through[11]

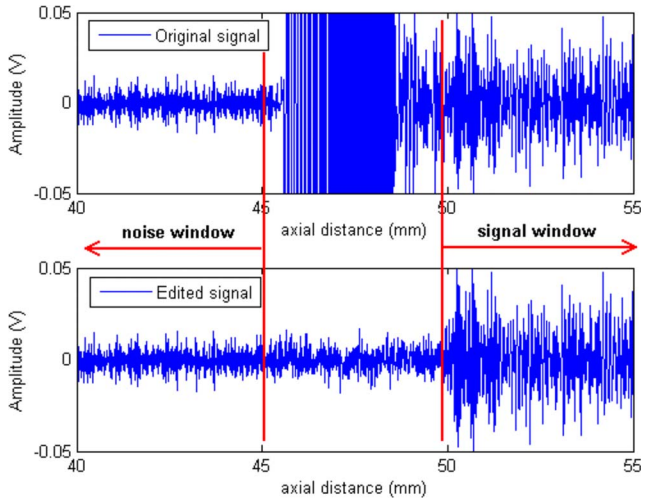

FIG. 3. (Color online) Front surface reflection replaced by zero-mean WGN.

$$\mathrm{eSNR} = 10 \log \frac{\sigma_s^2}{\sigma_n^2}, \tag{1}$$

where σ_s^2 and σ_n^2 are the variances of the signal from the scatterers and from a scatterer free region (noise), respectively. Figure 3 shows an example of the clipped chirp signal from the phantom surface and the clipped signal replaced by zero-mean WGN.

The system noise was much higher from the combined AWG and rf power amplifier system compared to the Panametrics 5800 pulser/receiver. Therefore, the eSNR was much higher for the pulse generation by using the Panametrics 5800 pulser/receiver (CP) than by using the rf power amplifier and AWG (CEPC). In order to quantify the benefits of increasing the eSNR through CEPC versus CP, the eSNR needed to be normalized between the CP signals and the coded excitation signals before pulse compression. To normalize the eSNR, zero-mean WGN was added to the CP signals.

Briefly, the variance of the system noise was estimated at a time window before the reflection of the front surface for the chirp setup. WGN was then created by using the randn( ) function in MATLAB, which creates normally distributed numbers with mean zero, variance 1. This was then multiplied with the square root of the estimated noise variance

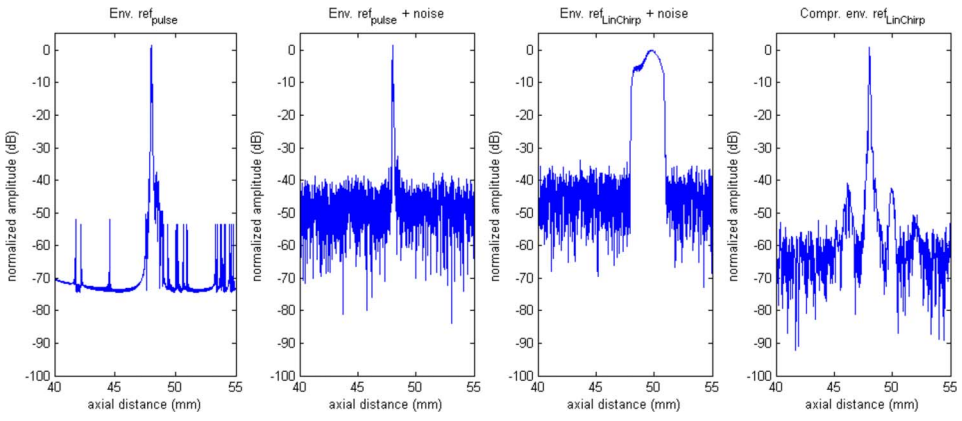

FIG. 4. (Color online) eSNR equalization through noise addition, shown for reference signals with pulsed and chirp signal. Also, the compressed signal is shown.

from the CEPC setup. This WGN was added to the data taken with the pulsed setup. For the signals taken as reflection of a planar surface in pulsed and chirp setup, the noise was created as well and added with the same algorithm. Figure 4 shows the envelopes of recorded signals reflected from a planar surface without and with noise added in comparison, for pulsed setup, and chirp setup before and after compression.

B. Backscatter coefficient estimation

A broadband substitution method valid for weakly focused transducers was used to estimate the backscatter coefficient. The backscatter coefficient σ_b was estimated from the normalized power spectral density (PSD) of the backscattered echo signal by

$$\sigma_b(f) = \frac{0.36(R_0 + R_1)^2}{A_0 \Delta z} W(f), \tag{2}$$

where A_0 is the area of the transducer.[6] $W(f)$ is the average PSD of the backscattered echo signals divided by the average PSD of the reference signal. Corrections for frequency-dependent attenuation and the reference spectrum were incorporated through

$$W(f) = \frac{1}{N_l} \sum_{l=1}^{N_l} \left(\frac{\gamma}{2}\right)^2 \frac{|S_m(f,Z_l)|^2}{|S_0(f,Z_l)|^2} e^{4\alpha_m(f)(R_1+(\Delta z)/2)}, \tag{3}$$

where N_l is the number of gated waveforms of length Z_l that have been obtained from the sample and γ is the amplitude reflection coefficient of the planar surface that was used to obtain the reference waveform. $S_m(f,Z_l)$ is the Fourier transform of the backscattered echo signal and $S_0(f,Z_l)$ is the Fourier transform of the reference signal. $\alpha_m(f)$ is the frequency-dependent attenuation coefficient of the sample medium. The frequency-dependent attenuation was estimated by using an insertion loss method. Briefly, the signal from a transducer was recorded with a hydrophone with and without the phantom material in between. The frequency-dependent attenuation was estimated by dividing the absolute value of the Fourier transforms of the signals with and without the phantom material and by the thickness of the phantom.[19,20] The backscattered echo signal waveforms were gated from regions of interest (ROIs) corresponding to inside the phantom by using a Hann window of width Δz.

C. Scatterer size estimation

The TM phantoms contained randomly located glass spheres of varying diameters, which were modeled by using established theory.[21,22] Specifically, theoretical backscatter coefficients versus frequency were calculated for different glass bead diameters (Fig. 5). The theoretical backscatter coefficients σ_{Faran} calculated for different diameters of glass beads were stored in a look up table (LUT) for faster processing speed. From the LUT, estimates of the glass bead diameter could be obtained by comparing the measured backscatter coefficients from the phantoms with σ_{Faran}. The estimated scatterer diameter was the value that minimized the average squared deviation (MASD) between the measured and theoretical backscatter coefficients given from the LUT.[23] The MASD is mathematically represented by

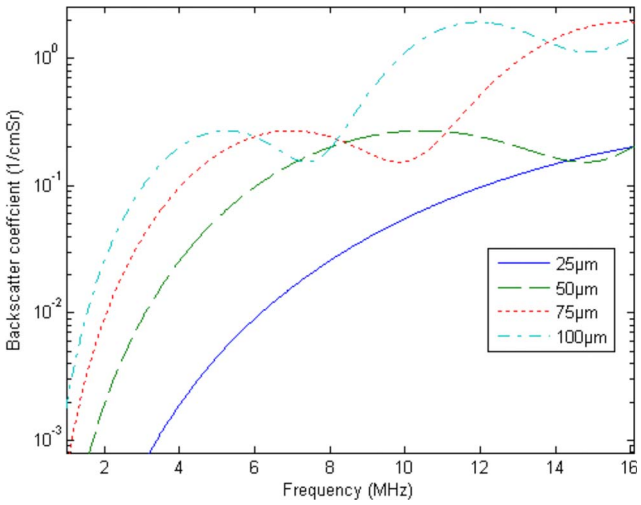

FIG. 5. (Color online) Calculated backscatter coefficient for glass beads with four different diameters vs frequency.

$$\text{MASD} = \min(\varepsilon\{(X(f,D) - \varepsilon\{X(f,D)\})^2\})_D, \tag{4}$$

with

$$X(f,D) = 10 \log_{10}\left(\frac{\sigma_b(f)}{\sigma_{\text{Faran}}(f,D)}\right). \tag{5}$$

$\varepsilon\{\cdots\}$ represents the mean and $X(f,D)$ is the ratio (decibels) of σ_b (in the −6 dB bandwidth of the transducer) to σ_{Faran} for the diameter D. By subtracting the mean $\varepsilon\{X(f,D)\}$ from $X(f,D)$, the result is independent from the magnitude of measured and calculated backscatter coefficients and only depends on the shape, i.e., the frequency dependence, of σ_b.[23]

At depths where the noise was much greater than the echo from the scatterers, the glass bead diameter estimates diverged from the median value. A rf spectrum dominated by white noise would have a slope of zero. After correcting for the frequency-dependent attenuation, the slope would take on the characteristics of the frequency-dependent attenuation correction. Likewise, for a band-limited signal, higher frequencies are attenuated more rapidly than lower frequencies, leading to lower SNR in the higher frequency channels. Compensating for frequency-dependent losses will result in an amplification of noise preferentially at higher frequencies in the analysis bandwidth. The amplification of noise will result in a larger slope for the estimated backscatter coefficient, which leads to an increasing bias in scatterer size estimates. The depth of penetration for obtaining reliable scatterer size estimates was defined to be the depth where the estimate bias (absolute difference between the median glass bead size and the estimated size) was less than 25%.

D. Coded excitation and pulse compression

For coded excitation, a linear FM chirp v was used as the excitation waveform. The chirp waveform was constructed using MATLAB (MathWorks, Natick, MA) and then uploaded to the AWG. The chirp had a center frequency

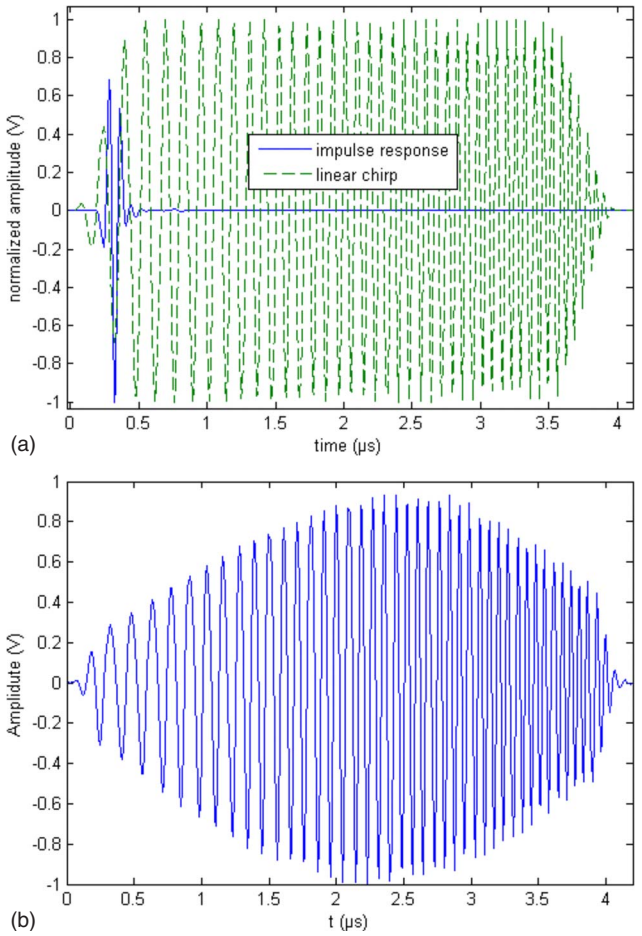

FIG. 6. (Color online) (a) Impulse response (solid line) of the 10 MHz transducer and the linear FM chirp (dashed line) used to excite the transducer. (b) Impulse response of the 10 MHz transducer excited with the linear FM chirp.

equal to the center frequency of the transducer and a time-bandwidth product (TBP) of 40. A TBP of 40 would lead to a gain in eSNR of 16 dB [10 log(TBP)] compared to conventional pulsing.[24] The bandwidth was chosen to be 1.14 times the −6 dB bandwidth of the transducer, which was determined to be the optimum bandwidth for a linear FM chirp.[25] Finally, the chirp was tapered using a 10% Tukey window to suppress sidelobe levels.

Figure 6 shows the impulse response of the 10 MHz transducer, the linear FM chirp used to excite the transducer (a), and the FM chirped signal measured from a planar reflector (b). The resulting sound waveform h_{out} was the convolution of the linear chirp with the impulse response of the system including the transducer. This waveform was propagated through the water and backscattered by the phantom. The received backscattered echo signals were compressed in MATLAB by convolution (or multiplication in frequency domain) with a filter function,

$$G_{pc} = G\beta, \tag{6}$$

where G is the Fourier transform of the received echo signal and β is the filter function. A Wiener filter was chosen because it allows the trade-offs between sidelobes and noise to be controlled. The Wiener filter is given by

TABLE I. Parameters of all four phantoms.

Parameter	Phantom A	Phantom B	Phantom C	Phantom D
Glass diameters (μm)	75–90	9–45	45–53	45–53
Speed of sound (m s^{-1})	1540	1540	1540	1540
Attenuation (dB MHz^{-1} cm^{-1})	0.5	0.7	0.5	0.7

$$\beta = \frac{V^*}{|V|^2 + \gamma_1 \overline{\text{eSNR}}^{-1}}, \tag{7}$$

where V is the Fourier transform of the excitation waveform and V^* designates its complex conjugate. $\overline{\text{eSNR}}$ is the average echo signal-to-noise ratio per frequency channel and is defined as

$$\overline{\text{eSNR}(u|x)} = \frac{|H(u|x)|^2 \varepsilon\{|F(u)|^2\}}{\varepsilon\{|E(u)|^2\}}, \tag{8}$$

where u is the discrete frequency sampling variable and $H(u|x)$, $F(u)$, and $E(u)$ are the Fourier transforms of $h(nT,x)$, $f(x)$, and $e[n]$, respectively.[26] $\varepsilon\{\cdots\}$ represents the expectation value, $e[n]$ is the noise present in the system, $h(nT,x)$ is the spatially varying impulse response of the system, and $f(x)$ is a function representing the scattering object. Because $f(x)$ is unknown for the sample, it is replaced by the average PSD of the gated waveforms divided by the PSD of h_{out},

$$|F(u)|^2 = \frac{\overline{|S_m(f,Z_l)|^2}}{|H_{\text{out}}(u|x)|^2}. \tag{9}$$

E. Test samples

In this study, four different test samples were used. All samples were fluidlike water-based agar materials that contained randomly positioned glass spheres (Potters Industries, Valley Forge, PA). Table I lists the relevant parameters associated with each of the TM phantoms used in this study.[19,20] The TM phantoms contained different concentrations of randomly located glass spheres. The sizes of glass spheres included in this study corresponded to scatterer sizes previously encountered in tissue experiments.[27] All phantoms where circular cylindrical samples with a diameter of 7.6 cm and a length of either 4 cm (phantoms A and B) or 5 cm (phantoms C and D). The phantoms were bounded on the curved surface with a plastic wall and on the flat surface with a 25-μm-thick Saran–Wrap plastic foil (Dow Chemical, Midland, MI).

The Saran–Wrap served as a window for transmitting ultrasound between the surrounding medium (water) and the TM material inside the phantom. To correct for the influence of the Saran–Wrap to the backscattered spectrum, the following equation was used:

$$T(k) = \frac{2Z_i}{2Z_i \cos(k_s * d)} + j\frac{1.69c_s + Z_i^2}{1.69c_s} \sin(k_s * d), \tag{10}$$

where k is the wave number represented by $2\pi f/c$, Z_i is the acoustic impedance (Z_i=14.9 kg m^{-2} s^{-1}), d is the thickness

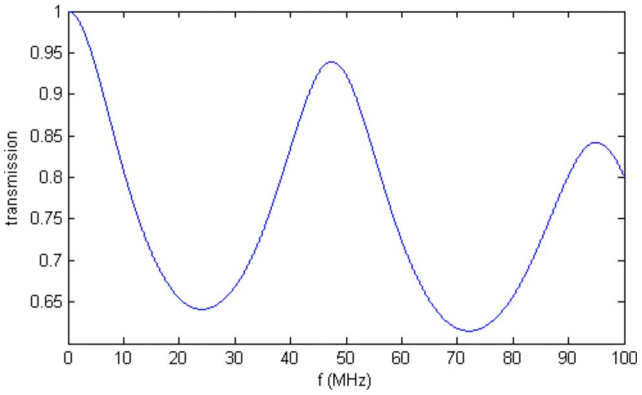

FIG. 7. (Color online) Transmission through two layers of 25-μm-thick Saran–Wrap.

of the Saran–Wrap layer (d=25.1 μm), c_s is the speed of sound inside the Saran–Wrap (c_s=2400 m s^{-1}), and k_s is the wave number inside the wrapping material,[19]

$$k_s = \frac{2\pi f}{c_s} - j(0.05f^{1.5}). \tag{11}$$

Figure 7 shows the transmission coefficient through two 25-μm-thick layers of Saran–Wrap. The backscatter coefficient was corrected for the frequency-dependent transmission through the Saran–Wrap layer by dividing $W(f)$ by the square of the power transmission coefficient (accounting for transmission in and out of the phantom).

III. EXPERIMENTAL RESULTS

The first set of data was obtained by using a weakly focused (f/3) 5 MHz single-element transducer (Panametrics, Waltham, MA) with a −6 dB bandwidth of 4.2 MHz. The linear FM chirp had a length of 8.9 μs and a bandwidth of 4.5 MHz, which led to a TBP of 40. The second set of data was obtained by using a weakly focused (f/4), single-element transducer (Panametrics, Waltham, MA) with a center frequency of 10 MHz and a −6 dB bandwidth of 9.1 MHz. The linear FM chirp had a length of 4 μs and a bandwidth of 10 MHz, which led to a TBP of 40 (an estimated gain in eSNR of 16 dB). A compression of the chirp waveforms from the planar reflector at the focus produced gains in eSNR of approximately 16 dB matching the expected increase. The eSNR gain can be observed in Fig. 4. All four phantoms were scanned 30 mm laterally with a step size of 0.5 mm. In addition, lateral scans were performed at three different distances. R_1 was set to 5, 10, and 15 mm, respectively. R_0 was decreased by the same amount that R_1 was increased, such that the sum of R_0 and R_1 was constant. This allowed for estimates to be obtained from deeper in the phantom while still within the depth of focus of the transducer. The axial length of the ROI Δz was set to 4 mm. The first 9 and 4 mm for the 5 and 10 MHz transducers, respectively, behind the front surface of the phantom was dominated by the chirp reflected from that surface. Therefore, the data sets used for analysis started at 10 or 5 mm behind the front surface.

TABLE II. *ka* ranges for three different scatterer diameters for 5 and 10 MHz measurements.

Average scattering diameter (μm)	*ka* range (5 MHz)	*ka* range (10 MHz)
25	0.12–0.34	0.28–0.75
49	0.24–0.66	0.54–1.45
82	0.40–1.10	0.91–2.45

The results at 5 MHz did not suggest an improvement in scatterer sizes estimates with depth. The reason for this lack of improvement is due to the lower attenuation of ultrasound at 5 MHz. While the gain in eSNR using CEPC over CP within the phantom was typically 10 dB or more, the eSNR for both CP and CEPC was always above 10 dB throughout the depth examined in each phantom. Therefore, at lower ultrasonic frequencies where attenuation is lower, the use of CEPC may not yield significant improvements in scatterer size imaging throughout the depth of field of the imaging source.

For the 10 MHz data, the maximum depth from which data was used was at 15 mm because signals from locations greater than 15 mm deep were already attenuated below the level of noise in the system. Figure 4 shows an example of the signal reflected from a planar surface with WGN added before and after compression. In the compressed image, it can be observed that the spatial resolution has been improved and the eSNR has been increased. The values of *ka* for the analysis bandwidth of the 5 and 10 MHz sources based on the estimated average scatterer radius are listed in Table II. Estimates of scatterer diameters were found to have the best performance in terms of bias and variance when the *ka* range went above 0.5. Figure 8 compares glass bead diameter estimates from ultrasound backscatter by using CP and CEPC from the phantom with the median value of glass bead diameter of 82 μm for CP and CEPC. A small absolute estimate bias is observed between the median value and the estimates by using CEPC at all depths, i.e., better than 25%. For CP, the estimates were close (less than 25% divergence) to the median value at depths smaller than 1.7 cm. The eSNR ranged from 0.1 to 1.6 dB for CP and 1.7 to 16 dB for

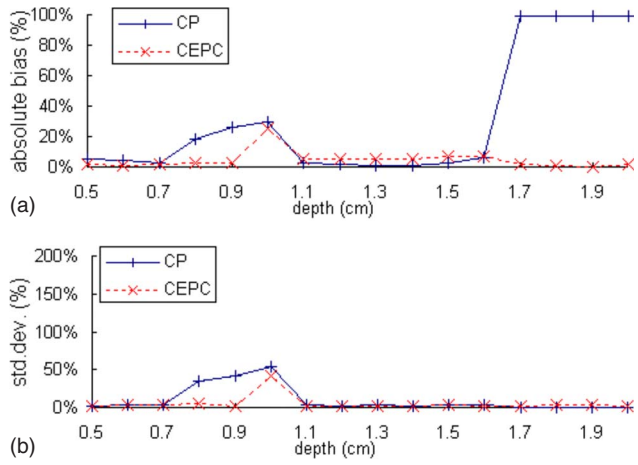

FIG. 8. (Color online) Phantom A: Estimated average scatterer sizes (plot a) and corresponding standard deviations (plot b) of 10 MHz measurements.

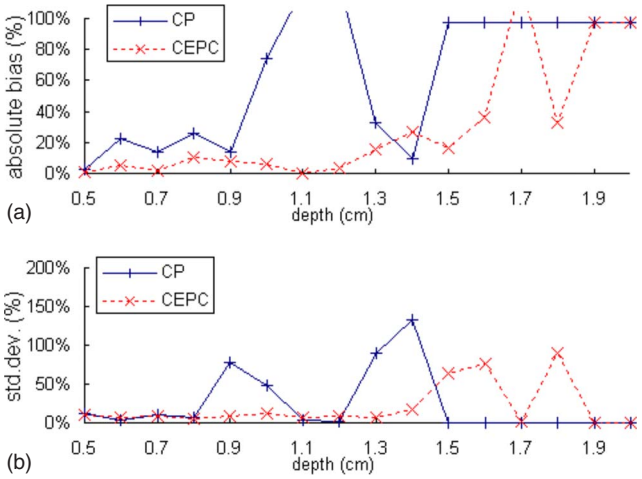

FIG. 9. (Color online) Phantom B: Estimated average scatterer sizes (plot a) and corresponding standard deviations (plot b) of 10 MHz measurements.

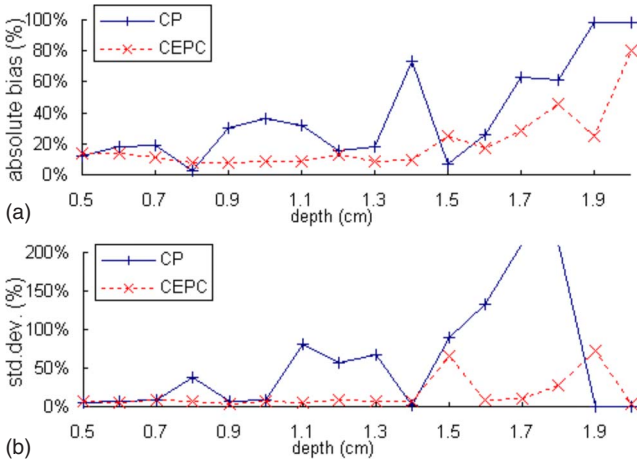

FIG. 11. (Color online) Phantom D: Estimated average scatterer sizes (plot a) and corresponding standard deviations (plot b) of 10 MHz measurements.

CEPC. At 1.7 cm, the eSNR was 0.2 dB (CP). For phantom B (Fig. 9), a bias to the calculated median glass bead diameter (25 μm) was observed. Estimates occurring closer to the surface, i.e., less than 1 cm, have an average estimated scatterer diameter of 40 μm. For a distribution of sizes in the phantom material, scatterer size estimates will be larger than the median value because the backscatter coefficient is proportional to the size of the scatterer to the sixth power. Because the range of glass bead diameters in phantom B is large, i.e., 9–45 μm, an average estimate of 40 μm is reasonable. By using 40 μm as reference value, good estimates were obtained for depths smaller than 1.0 and 1.5 cm for CP and CEPC, respectively. At these depths, estimates started to diverge from the reference value by more than 25% and the standard deviations increased above 70%. eSNR values ranged from 0 to 1.6 dB for CP and from 0 to 16 dB for CEPC. Moreover, at the diverging point, the eSNR was 0.5 dB for CP and 2.4 dB for CEPC. Diverging point is defined as the point in depth, where the deviations from the reference value or the error in the estimates where too high (>25% error). Therefore, the diverging point for CP is considered to occur at 1.0 cm even though the estimate bias appears to decrease between the depths of 1.2–1.4 cm. However, at a depth of 1.2 cm, the estimate bias is well above 100%, and at the depths of 1.3 and 1.4 cm, the standard deviations are above 100%. A similar behavior was observed from phantoms C and D. From phantom C (Fig. 10), CEPC produced accurate estimates until 1.6 cm depth was reached; the eSNR was 5.7 dB at this point. CP only produced accurate estimates in depths smaller than 1.1 cm, where eSNR was larger than 0.5 dB. eSNR values ranged from 0 to 1.8 dB for CP and from 1.2 to 16 dB for CEPC. Similar responses were observed from phantom D (Fig. 11), however, the diverging points occurred at different positions. The estimates were close to the median value (better than 25%) in depths smaller then 1 cm when CP was used and in depths smaller than 1.8 cm when CEPC was used. Again, it was observed that close to the diverging point, the standard deviations significantly increased. eSNR values were 0.6 dB for CP and 1.7 dB for CEPC at the diverging point. Table III summarizes the value of depth at which the bias begins to diverge and the eSNR value where the divergence occurs.

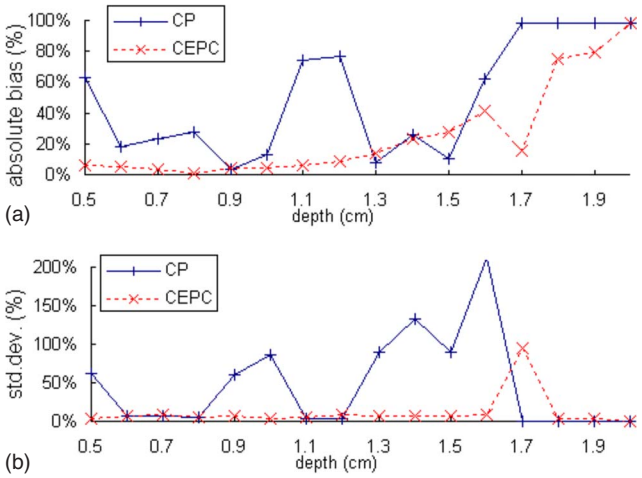

FIG. 10. (Color online) Phantom C: Estimated average scatterer sizes (plot a) and corresponding standard deviations (plot b) of 10 MHz measurements.

IV. DISCUSSION AND CONCLUSIONS

For the 5 MHz measurements, no significant differences in the estimated scatterer diameters were observed between the CP method and the CEPC method. This was due to larger eSNR available throughout the depth of phantom when using 5 MHz. This was not the case for the 10 MHz data, where the attenuation quickly attenuated the signal, resulting in decrease in the ability to accurately estimate scatterer size. The

TABLE III. Summary of estimate results at the 25% bias divergence by using 10 MHz.

	Bias depth (cm)		eSNR (dB)	
Phantom	CP	CEPC	CP	CEPC
A	1.7	2.0	0.19	1.74
B	1.0	1.6	0.35	1.48
C	1.1	1.6	0.42	4.68
D	1.0	1.8	0.52	1.64

use of CEPC at 10 MHz resulted in a significant increase in penetration depth yielding accurate estimates and provided the ability to estimate the correct diameter of the scattering objects in regions where the CP method failed. When comparing the results of phantom A, a gain in penetration depth of at least 0.4 cm was obtained when CEPC was used instead of CP. If a greater depth was examined with phantom A at 10 MHz, the increase in depth of penetration may have been even larger. When comparing the results of phantoms B, C, and D, the gain in penetration depth was about 50% (7, 6, and 8 mm, respectively) when CEPC was used instead of CP.

Any improvement in estimate variance when using CEPC was found to be modest at best; however, it can be concluded that the use of CEPC did not cause the estimate variance to become worse. Variance in scatterer size estimates is driven by electronic noise at low eSNR and by spatial variation noise due to the random location of scatterers in the phantoms.[28] While coded excitation can increase the eSNR related to electronic noise, it cannot reduce the spatial variation noise (the scatterers are still located spatially at random).

The comparison of CP and CEPC suggests that for the 10 MHz measurements, where the eSNR was crucial for the success of the estimations, using CEPC yielded significant benefits. This is highlighted by the fact that CEPC was more successful than CP in deeper regions of the phantoms, where the attenuation was high and the amplitude of the noise was much higher than the amplitude of the signal, even after averaging. The expected gain in penetration depth when CEPC was used led to a higher eSNR, which improved the bias and variance of estimates.

When analyzing the tissue, the attenuation of the ultrasound decreases eSNR with the depth of the ROI and with an increase in the center frequency. In order to keep good measurement conditions in terms of scatterer diameter and frequency ($ka > 0.5$), it is often necessary to use higher frequencies when the scatterers are relatively small. The use of higher frequencies leads to higher attenuation and the need for increasing the eSNR. When coded excitation is used in clinical ultrasound, the eSNR can be safely increased without exceeding the regulatory limits and with pulse compression the spatial resolution can be preserved.

The current study suggests that it is possible to use CEPC when estimating the average diameter of scatterers by measuring backscatter coefficients inside TM phantoms. One advantage of using CEPC over CP techniques was the improvement in accuracy of scatterer diameter estimates in measurement scenarios where the level of attenuation was high enough such that the eSNR was below 1 dB. More important, accurate scatterer diameter estimates were obtained for low eSNR signals, indicating that the ability to estimate scatterer properties is robust. A second advantage was the improvement in variance for estimates by using CEPC over CP. While the improvement in estimate variance was small, it was still quantifiable and will improve the ability to distinguish tissue types using scatterer size imaging.

Although the penetration depth for scatterer size imaging was increased in the phantom studies, the gain was less than predicted. For example, the gain in eSNR by using CEPC was 14–15 dB. If the attenuation was 0.7 dB MHz^{-1} cm^{-1}, then at 10 MHz the loss per centimeter of penetration is 7 dB. Therefore, for CEPC, the expected gain in penetration depth should be a full 2 cm. The largest gain in the experimental results was 0.8 cm, less than half the gain that would be predicted by the increase in eSNR. The reason for this discrepancy may be due to the analysis bandwidth being used. While 10 MHz is the center frequency of the source, the actual bandwidth used includes both lower and higher frequencies. Therefore, the loss of the higher frequencies, which attenuate more rapidly, may cause the bias to the estimate to increase earlier in the phantom. The *ka* range due to the decreasing analysis bandwidth will become smaller and may reduce below 0.5. Low *ka* values correspond to a decreased ability to accurately estimate the scatterer size because the frequency dependence of scattering is not greatly affected by scatterer size at low *ka*.[23]

In future studies, other structural properties of tissue derived from the backscatter coefficients, i.e., scatterer concentration, could be examined by using CEPC. CEPC will be an important tool to analyze tissue by measuring the backscatter coefficient and estimating structural properties, especially when the scatterers are relatively small and higher frequencies have to be used to have a *ka* above 0.5. This could have a significant impact in tissue characterization of superficial cancer sites, e.g., the thyroid, breast, testes, or prostate, where higher frequencies may reveal more detail and important microstructure related to scattering from cells.[27] Future studies will also examine the effects of side lobes on scatterer property estimates, the effects of ROI size on estimate variance and bias by using CEPC, and application of CEPC and quantitative ultrasound to animal models in cancer detection.

Finally, the frequency modulated coded excitation was evaluated for improving the estimation of scatterer size. However, the use of phase based codes, e.g., Golay or Barker codes, could also be used to improve scatterer size estimates with similar expected benefits. Future work will examine the use of alternate coding schemes to improve the penetration depth of scatterer size imaging.

ACKNOWLEDGMENTS

The authors would like to acknowledge the helpful discussions and technical assistance of J. Sanchez, R. Lavarello, A. Haak, and A. Thakkar. This work was supported by a grant from the NIH (Grant No. R21 EB006741).

[1] J. G. Miller, J. E. Perez, J. G. Mottley, E. I. Madaras, P. H. Johnston, E. D. Blodgett, L. J. Thomas, III, and B. E. Sobel, "Myocardial tissue characterization: An approach based on quantitative backscatter and attenuation," Ultrason. Symp. Proc. **2**, 782–793 (1983).
[2] F. L. Lizzi, M. Greenebaum, E. J. Feleppa, M. Elbaum, and D. J. Coleman, "Theoretical framework for spectrum analysis in ultrasonic tissue characterization," J. Acoust. Soc. Am. **73**, 1366–1373 (1983).
[3] F. L. Lizzi, M. Ostromogilsky, E. J. Feleppa, M. C. Rorke, and M. M. Yaremko, "Relationship of ultrasonic spectral parameters to features of tissue microstructure," IEEE Trans. Ultrason. Ferroelectr. Freq. Control **34**, 319–329 (1987).
[4] M. F. Insana, T. J. Hall, and J. L. Fishback, "Identifying acoustic scattering sources in normal renal parenchyma from the anisotropy in acoustic properties," Ultrasound Med. Biol. **17**, 613–626 (1991).
[5] M. L. Oelze, J. F. Zachary, and W. D. O'Brien, Jr., "Characterization of

tissue microstructure using ultrasonic backscatter: Theory and technique optimization using a Gaussian form factor," J. Acoust. Soc. Am. **112**, 1202–1211 (2002).
[6]M. F. Insana and T. J. Hall, "Parametric ultrasound imaging from backscatter coefficient measurements: Image formation and interpretation," Ultrason. Imaging **12**, 245–267 (1990).
[7]M. F. Insana and D. G. Brown, "Acoustic scattering theory applied to soft biological tissues," in *Ultrasonic Scattering in Biological Tissues*, edited by K. K. Shung and G. A. Thieme (CRC, Boca Raton, FL, 1993), pp. 75–124.
[8]E. J. Feleppa, T. Liu, A. Kalisz, M. C. Shao, N. Fleshner, V. Reuter, and W. R. Fair, "Ultrasonic spectral-parameter imaging of the prostate," Int. J. Imaging Syst. Technol. **8**, 11–25 (1997).
[9]F. L. Lizzi, M. Astor, T. Liu, C. Deng, D. J. Coleman, and R. H. Silverman, "Ultrasonic spectrum analysis for tissue assays and therapy evaluation," Int. J. Imaging Syst. Technol. **8**, 3–10 (1997).
[10]A. Nair, B. D. Kuban, N. Obuchowski, and D. G. Vince, "Assessing spectral algorithms to predict atherosclerotic plaque composition with normalized and raw intravascular ultrasound data," Ultrasound Med. Biol. **27**, 1319–1331 (2001).
[11]J. Liu and M. F. Insana, "Coded pulse excitation for ultrasonic strain imaging," IEEE Trans. Ultrason. Ferroelectr. Freq. Control **52**, 231–240 (2005).
[12]A. V. Oppenheim and R. W. Schafer, *Digital Signal Processing* (Prentice-Hall, Englewood Cliffs, NJ, 1975).
[13]J. F. Zachary, J. M. Sempsrott, L. A. Frizzell, D. G. Simpson, and W. D. OBrien, Jr., "Superthreshold behavior and threshold estimation of ultrasound-induced lung hemorrhage in adult mice and rats," IEEE Trans. Ultrason. Ferroelectr. Freq. Control **48**, 581592 (2001).
[14]M. L. Oelze and W. D. O'Brien, Jr., "Application of three scattering models to the characterization of solid tumors in mice," Ultrason. Imaging **28**, 83–96 (2006).
[15]N. A. H. K. Rao, "Investigation of a pulse compression technique for medical ultrasound: A simulation study," Med. Biol. Eng. Comput. **32**, 181–188 (1994).
[16]C. E. Cook and W. M. Siebert, "The early history of pulse compression radar," IEEE Trans. Aerosp. Electron. Syst. **24**, 825–833 (1988).
[17]B. Haider, P. A. Lewis, and K. E. Thomenius, "Pulse elongation and deconvolution filtering for medical ultrasound imaging," IEEE Trans. Ultrason. Ferroelectr. Freq. Control **45**, 98–113 (1998).
[18]K. Raum and W. D. O'Brien, Jr., "Pulse-echo field distribution measurement technique of high-frequency ultrasound sources," IEEE Trans. Ultrason. Ferroelectr. Freq. Control **44**, 810–815 (1997).
[19]K. A. Wear, T. A. Stiles, G. R. Frank, E. L. Madsen, F. Cheng, E. J. Feleppa, C. S. Hall, B. S. Kim, P. Lee, W. D. O'Brien, Jr., M. L. Oelze, B. I. Raju, K. K. Shung, T. A. Wilson, and J. R. Yuan, "Interlaboratory comparison of ultrasonic backscatter coefficient measurements from 2 to 9 MHz," J. Ultrasound Med. **24**, 1235–1250 (2005).
[20]E. Madsen, F. Dong, G. R. Frank, B. S. Garra, K. A. Wear, T. Wilson, J. A. Zagzebski, H. L. Miller, K. K. Shung, S. H. Wang, E. J. Feleppa, T. Liu, W. D. O'Brien, Jr., K. A. Topp, N. T. Sanghvi, A. V. Zaitsev, T. J. Hall, J. B. Fowlkes, O. D. Kripfgans, and J. G. Miller, "Interlaboratory comparison of ultrasonic backscatter: Attenuation, and speed measurements," J. Ultrasound Med. **18**, 615–631 (1999).
[21]J. J. Faran, "Sound scattering by solid cylinders and spheres," J. Acoust. Soc. Am. **23**, 405–418 (1951).
[22]R. Hickling, "Analysis of echoes from a solid elastic sphere in water," J. Acoust. Soc. Am. **34**, 1582–1592 (1962).
[23]M. F. Insana, R. F. Wagner, D. G. Brown, and T. J. Hall, "Describing small-scale structure in random media using pulse-echo ultrasound," J. Acoust. Soc. Am. **78**, 179–192 (1990).
[24]M. L. Oelze, "Bandwidth and resolution enhancement through pulse compression," IEEE Trans. Ultrason. Ferroelectr. Freq. Control **54**, 768–781 (2007).
[25]M. Pollakowski, H. Ermert, L. von Bernus, and T. Schmeidl, "The optimum bandwidth of chirp signals in ultrasonic applications," Ultrasonics **31**, 417–420 (1993).
[26]J. K. Tsou, J. Liu, and M. F. Insana, "Modeling and phantom studies of ultrasonic wall shear rate measurements using coded pulse excitation," IEEE Trans. Ultrason. Ferroelectr. Freq. Control **53**, 724–734 (2006).
[27]M. L. Oelze and J. F. Zachary, "Examination of cancer in mouse models using high-frequency quantitative ultrasound," Ultrasound Med. Biol. **32**, 1639–1648 (2006).
[28]M. L. Oelze and W. D. O'Brien, Jr., "Defining optimal axial and lateral resolution for estimating scatterer properties from volumes using ultrasound backscatter," J. Acoust. Soc. Am. **115**, 3226–3234 (2004).